Clim. Past, 17, 2291–2303, 2021
https://doi.org/10.5194/cp-17-2291-2021

Climate of the Past
Open Access
EGU

Different facets of dry–wet patterns in south-western China over the past 27 000 years

Mengna Liao[1,★], **Kai Li**[1,★], **Weiwei Sun**[2], **and Jian Ni**[1]

[1]College of Chemistry and Life Sciences, Zhejiang Normal University, Jinhua, PR China
[2]State Key Laboratory of Lake Science and Environment, Nanjing Institute of Geography and Limnology, Chinese Academy of Sciences, Nanjing, PR China
★These authors contributed equally to this work.

Correspondence: Jian Ni (nijian@zjnu.edu.cn)

Received: 14 May 2021 – Discussion started: 3 June 2021
Accepted: 12 September 2021 – Published: 29 October 2021

Abstract. Frequently occurring mega-droughts under current global climate change have attracted broad social attention. A paleoclimatic perspective is needed to increase our understanding of the causes and effects of droughts. Southwestern (SW) China has been threatened by severe seasonal droughts. Our current knowledge of millennial-scale dry and wet phases in this region is primarily based on the variability of the Indian summer monsoon. However, water availability over land does not always follow patterns of monsoonal precipitation but also depends on water loss from evaporation and transpiration. Here, we reconstructed precipitation intensity, lake hydrological balance and the soil water stress index (SWSI) for the last 27 000 years. Grain size, geochemical and pollen records from Yilong Lake reveal the long-term relationships and inconsistencies of dry–wet patterns in meteorological, hydrological and soil systems in the central Yunnan region, SW China. Our results show that the long-term trends among precipitation, hydrological balance and soil moisture varied through time. The hydrological balance and soil moisture were primarily controlled by temperature-induced evaporation change during periods of low precipitation such as the Last Glacial Maximum and Younger Dryas. During periods of high precipitation (the early to late Holocene), intensified evaporation from the lake surface offset the effects of increased precipitation on the hydrological balance. However, abundant rainfall and the dense vegetation canopy circumvented a soil moisture deficit that might have resulted from rising temperature. In conclusion, the hydrological balance in the central Yunnan region was more sensitive to temperature change while soil moisture could be further regulated by vegetation changes over millennial timescales. Therefore, under future climate warming, the surface water shortage in the central Yunnan region may become even more serious. Our study suggests that reforestation efforts may provide some relief to soil moisture deficits in this region.

1 Introduction

The global land area experiencing extreme-to-exceptional terrestrial water storage drought could more than double by the late twenty-first century (Pokhrel et al., 2021). In southwestern (SW) China, drought has become a climate threat which is likely to happen more frequently in the future (Qiu, 2010; Wang et al., 2016). It is generally thought that long-term dry and wet phases in SW China are primarily regulated by the intensity of monsoonal precipitation associated with the evolution of atmospheric circulation systems (Chen et al., 2014; Hillman et al., 2017; Sun et al., 2019; Wang et al., 2019). However, drought refers to the amount of water available in both the soil and hydrological systems, which are dependent on precipitation and a range of other factors. These include how much water is able to infiltrate to deeper ground layers or is lost as runoff, and how much is evaporated directly from water and soil surfaces, or transpired by plants (Breshears et al., 2005; Dai et al., 2018; Feng and Liu, 2015; Mishra and Singh, 2010; Trenberth et al., 2014). Therefore, drought does not only happen during periods of low precipitation (Dai et al., 2018; Sun et al., 2017; Trenberth et al., 2014; Xu et al., 2019). Given this, understanding dry–

wet patterns in different climate scenarios while considering physical and vegetation processes is crucial to predicting the future risk of drought.

Climate evolution in SW China since the Last Glacial Maximum (LGM) has been reconstructed using various types of paleoclimatic archives, such as speleothem oxygen isotope records (e.g. Cai et al., 2015; Dykoski et al., 2005; Zhao et al., 2015), lake sediments (e.g. Hillman et al., 2017, 2020; Hodell et al., 1999; Li et al., 2018; Sun et al., 2019; Wang et al., 2020; Wu et al., 2018; Xiao et al., 2014a, b; Zhang et al., 2017; E. Zhang et al., 2019), and peats (e.g. Huang et al., 2016; Wei et al., 2012). The major conclusion of these studies is that monsoonal precipitation and temperature was very low during the LGM, and precipitation peaked in the early Holocene during a period of warmer climate, before both precipitation and temperature declined. The "cold–dry" and "warm–humid" paradigms of climate change in SW China have been widely demonstrated from a paleoclimatological perspective, despite the proposition that summer temperature and monsoon precipitation were decoupled in the early Holocene (Wu et al., 2018). Additionally, vegetation in SW China has experienced noticeable changes since the LGM (Chen et al., 2014; Cook et al., 2011; Wu et al., 2018; Xiao et al., 2014a, b), which may have affected evapotranspiration processes. Since water availability is a tradeoff among precipitation input and water loss through evaporation, transpiration and outflow (Breshears et al., 2005; Dai et al., 2018; Watras et al., 2014), these processes may lead to different environmental signatures of the wet and dry patterns over land. However, to our knowledge few studies have tested this idea.

Definitions of "drying" in meteorology, hydrology and biology are different but connected (Mishra and Singh, 2010). In paleoclimatology, drying or moistening processes can be reconstructed by different types of proxies, but the concepts underpinning them are not necessarily the same. For example, grain-size records from several lakes in SW China reflected variations in Indian summer monsoon (ISM) precipitation (Ning et al., 2017; Peng et al., 2019; Sheng et al., 2015). Authigenic carbonate precipitation is strongly affected by the hydrological balance or precipitation–evaporation ratio (Leng and Marshall, 2004; Ohlendorf et al., 2013) and thus indicates changing hydrological conditions in lake-catchment systems. For terrestrial ecosystems, soil water is the main and direct source of water for most plants and a primary constraint for vegetation composition and biomass. Consequently, changes in the soil moisture can theoretically be reflected in pollen records. As yet, soil moisture status has rarely been reconstructed using pollen data, and the similarities and differences between the dry–wet patterns revealed from different paleoproxies are seldom discussed.

The Yunnan region is located in the south-west of China (Fig. 1). It is primarily influenced by warm and humid airflow from the Bay of Bengal in summer. Several paleolimnological studies have shown that, since the LGM or the Holocene, precipitation, hydrological conditions and vegetation in the Yunnan region has experienced noticeable changes (Hillman et al., 2017, 2020; Hodell et al., 1999; Ning et al., 2017; Sun et al., 2019; Wu et al., 2018; Xiao et al., 2014a). However, few studies have applied a multi-proxy approach at the same temporal scale to explore different aspects of the long-term dry–wet patterns. Here we have developed the first record of a soil water stress index (SWSI) based on a pollen record from Yilong Lake in the Yunnan region to reveal changes in soil moisture over the past 27 000 years. By comparing the SWSI reconstruction with records of monsoonal precipitation and hydrological balance in the same core, we aim to discuss the long-term relationships of dry–wet patterns in the meteorological, hydrological and soil systems in SW China.

2 Materials and methods

2.1 Study site and modern climate

Yilong Lake (23.63–23.70° N, 102.50–102.65° E, 1414 m a.s.l.) is a faulted lake in the central Yunnan region, SW China (Fig. 1a). It covers an area of 38 km^2 and has a catchment area of 303.6 km^2 (Wang and Dou, 1998). The average water depth is 2.8 m and the maximum is 6.2 m (Wang and Dou, 1998). Yilong Lake is a freshwater lake which is fed by overland runoff, lake surface precipitation and groundwater. All the inflowing rivers, except the Chenghe River at the north-west of the Lake, are seasonal (Fig. 1b). An outlet was located at the south-east end of the lake during past highstands, but it disappeared in 1978 CE due to climate- and human-induced lower lake levels (Wang and Dou, 1998).

The central Yunnan region is dominated by a subtropical monsoon climate. Observations from the closest meteorological station in Yuxi City (24.2° N, 102.338° E, 1717 m a.s.l.), 80 km away from Yilong Lake, record a mean annual temperature of 18.1 °C after lapse rate correction (0.65 °C per 100 m) and mean annual precipitation of 886 mm (1951–2017 CE; China Meteorological Data Service Centre, https://data.cma.cn/en, last access: 26 March 2021). Annual evaporation (1035 mm) in this region is slightly higher than the annual precipitation. Seasonal climate change is characterised by high precipitation in the warm season with low precipitation in the cold season (Fig. 1c).

2.2 Sampling and dating

In May 2017, a sediment core (YLH) was retrieved from Yilong Lake at a water depth of 4.1 m (Fig. 1b) using a UWITEC sampling system. The sediment core was transported to the Nanjing Normal University's School of Geography laboratory and kept at 3.9 °C until analysis. The sediment core was split with a Geotek Core Splitter, photographed and visually described in the laboratory. The samples were sub-

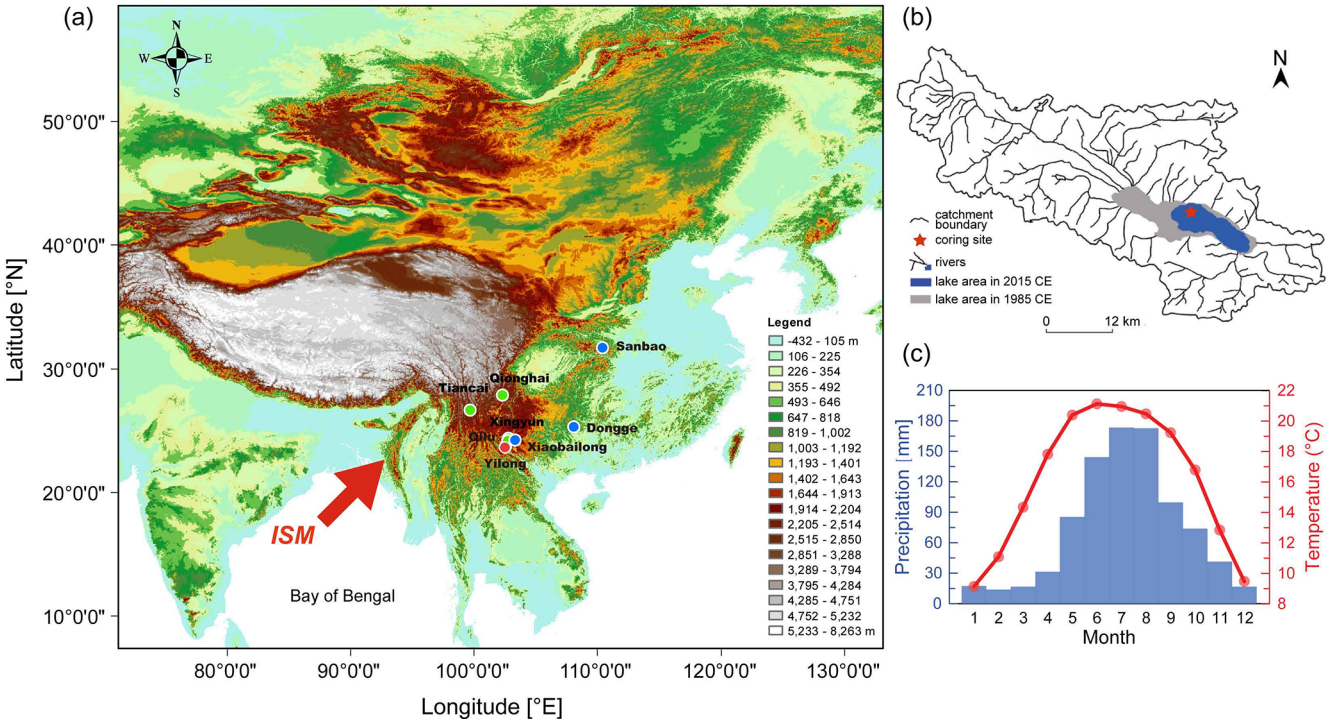

Figure 1. **(a)** Map showing the location of Yilong Lake and other paleoclimatic records; **(b)** catchment of the lake and the location of the core YLH; **(c)** average monthly temperature and precipitation from 1951 to 2017 CE (China Meteorological Data Service Centre, https://data.cma.cn/en, last access: 26 March 2021).

sampled at 1 cm intervals, freeze-dried and used for further analyses.

The age of the core YLH was determined using 15 accelerator mass spectrometry (AMS) ^{14}C dates including bulk organic matter, charcoal and plant remains (Table 1). ^{14}C dates were analysed by the Beta Analytic Testing Laboratory. The conventional ^{14}C dates were calibrated using Calib 8.20 with an IntCal20 calibration dataset (Reimer et al., 2020). Age–depth modelling was performed in R (version 3.4.4, R Core Team, 2018) using the package "rbacon" (Blaauw et al., 2020). According to the age–depth model, the basal sediment was deposited between 27.171–26.439 ka cal BP with a median age of 26.866 ka cal BP (Fig. 2).

2.3 Analytical methods

Samples for grain size analysis were measured at 1 cm intervals. All samples were pretreated with 30 % H_2O_2 and then 5 % HCl to remove organic matter and carbonates, rinsed with deionised water to neutralise the samples, and placed in an ultrasonic bath with 10 % $(NaPO_3)_6$ added to disperse particles. The grain size distribution was measured by a Malvern 3000E laser diffraction instrument with 100 bins ranging from 0.02 to 2000 µm.

The sediments (collected at 1 cm intervals) were pretreated with 10 % HCl to remove carbonates and then used to measure the total organic carbon (TOC) and total nitrogen (TN) using a vario EL cube elemental analyser. Replicate analyses of well-mixed samples showed that the precision was ca. $\pm < 0.1$ % (1 standard deviation (SD)). Continuous down-core X-ray fluorescence (XRF) measurements of the geochemical composition were carried out with a core scanner (MSCL-S – specifications: tube voltage 15 kV, exposure time 30 s and spatial distribution 0.5) at the laboratory of the School of Geography, Nanjing Normal University. The sample moved along a monochromatized and polarised SR beam. Core scanning started from 10 cm depth as the upper 10 cm of sediments has a high water content and is too soft to get robust measurements. Core bulk mineralogy of freeze-dried and milled samples (at 2 cm intervals) was measured by X-ray diffraction (XRD) using a PANalytical X'pert Pro (40 kV, 30 mA, from 5–80°, step rate 0.0167°, Cu kα radiation) at the Qinghai Institute of Salt Lakes, Chinese Academy of Science (CAS). A total of 71 freeze-dried samples from depths where carbonate content is (relatively) high (10–176 and 228–280 cm) were measured for oxygen stable isotopes in carbonate ($^{18}O_{carb}$) using a Thermo-Fisher MAT 253 mass spectrometer equipped with a Kiel-IV carbonate preparation device at the Nanjing Institute of Geography and Limnology, CAS. The samples were pretreated with 100 % phosphoric acid. The $^{18}O_{carb}$ values are expressed as standard delta (δ) notation as the per mill (‰) deviation from Vienna Pee Dee Belemnite (VPDB). Four samples at different depths were

Table 1. AMS ^{14}C results from the YLH sediment core.

Lab ID	Depth [cm]	Materials	IRMS $\delta^{13}C$ [‰]	Conventional radiocarbon age [BP]	Calibrated age [2σ, cal BP]
Beta-468347	1	Sediment TOC	24.6	-30 ± 30	100.37 ± 0.37 pMC
Beta-492284	40	Charcoal and plant remains	−21.5	2820 ± 30	2848–3004
Beta-492285	80	Charcoal and plant remains	−20	4820 ± 30	5477–5539
Beta-468348	91	Sediment TOC	−27.3	5560 ± 30	6297–6398
Beta-492286	140	Charcoal and plant remains	−18.7	6330 ± 30	7237–7318
Beta-468349	170	Charcoal and plant remains	−21.5	7510 ± 30	8289–8386
Beta-492287	180	Charcoal and plant remains	−28.7	7860 ± 30	8585–8771
Beta-492288	230	Charcoal and plant remains	−13.1	$12\,460 \pm 40$	14 322–14 745
Beta-468350	255	Sediment TOC	−17.6	$13\,880 \pm 40$	16 678–17 025
Beta-492289	280	Sediment TOC	−18.8	$14\,800 \pm 40$	17 986–18 242
Beta-468351	325	Sediment TOC	−19.9	$16\,400 \pm 50$	19 582–19 923
Beta-541605	338	Plant remains	−27	$16\,730 \pm 50$	20 058–20 408
Beta-468352	383	Sediment TOC	−19.3	$21\,980 \pm 70$	25 973–26 393
Beta-537522	404	Charcoal	−25.1	$20\,320 \pm 70$	24 183–24 631
Beta-468353	457	Plant remains	−17.8	$22\,560 \pm 80$	26 829–27 171

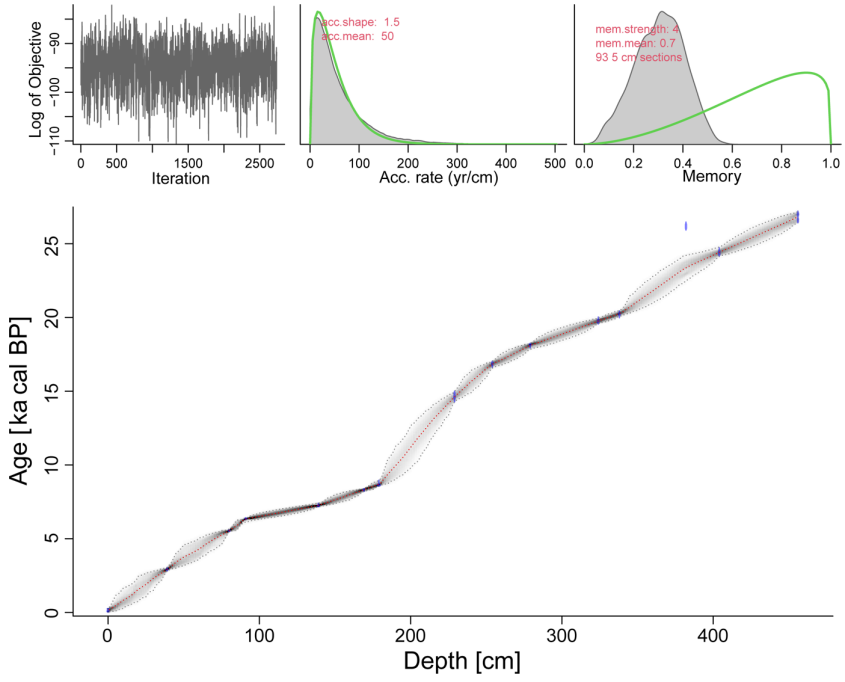

Figure 2. Age–depth model of the sediment core YLH.

imaged using a Hitachi SU8010 scanning electron microscope (SEM) to examine crystal structure and morphology of carbonate minerals.

Samples for pollen analysis were analysed at 4 cm intervals and treated with standard laboratory methods (Faegri et al., 1989), including treatment with 10 % HCl and 50 % HF to remove carbonates and silicates, boiling in 10 % KOH to remove humic acid, sieving to remove the fine and coarse fractions, and mounting in silicone oil. To calculate the concentrations of pollen, tablets containing a known quantity of *Lycopodium* spores were added to each sample prior to the treatments. At least 300 terrestrial pollen grains per sample were counted. All the treatment and identification was processed in the Institute of Hydrogeology and Environmental Geology, Chinese Academy of Geological Sciences. The pollen percentages were calculated based on the total number of pollen grains from terrestrial pollen taxa and used to construct a pollen diagram and conduct numerical analyses.

2.4 Pollen-based quantitative reconstruction of SWSI

In total, 1394 surface soil pollen samples from SW China (Ni et al., 2014; Fig. S1 in the Supplement) were used in this study. Annual climate data were averaged from long-term records from 1971 to 2000 at 1814 meteorological stations across China (China Meteorological Data Service Centre, https://data.cma.cn/en Last access date: 22 May 2003). These data were interpolated into 1 km grid cells using a thin-plate smoothing-spline surface fitting technique (Hancock and Hutchinson, 2006) that takes the impact of elevation into account on the basis of the Shuttle Radar Topography Mission (SRTM) digital elevation model (Farr et al., 2007). The interpolation was performed in the program ANUSPLIN version 4.36 (Hutchinson, 2006). The interpolated meteorological data were used to calculate the SWSI using the SPLASH v.1.0 program (Davis et al., 2017). SWSI reflects the degree of evapotranspiration deficit and is expressed as (PET−AET)/PET, where AET and PET are the annual sums of actual and potential evapotranspiration, respectively (Prentice et al., 1993). The SWSI reconstruction was calculated using the weighted-averaging partial least square (WA-PLS) regression (ter Braak and Juggins, 1993). The pollen percentages were square-root transformed to stabilise variances and optimise the signal-to-noise ratio (Prentice, 1980). The "leave-one-out" cross-validation was used to test the reliability and robustness of the model. The number of components to include in the transfer function was selected as those producing the lowest root mean squared error of prediction (RMSEP), a high coefficient of determination between observed and predicted environmental values (r^2), and low average bias (ter Braak and Juggins, 1993). These analyses were carried out using R package "rioja" (Juggins, 2017).

3 Results

3.1 Grain size and geochemical data of core YLH

Grain size in core YLH are mainly composed of clay (< 4 µm) and silt (4–63 µm), with mean contributions of 25 % and 70.2 %, respectively. Down-core variations of the clay component exhibit generally high values during ca. 16–27.5 ka cal BP (ca. 246–456 cm) and ca. 0–3 ka cal BP (ca. 0–40 cm), and low values with strong fluctuations during ca. 3–16 ka cal BP (ca. 41–245 cm) (Fig. 3). The variations of the silt component are generally opposite to that of the clay component. The sand component is characterised by low percentages throughout the core (average percentage of 4.8 %), punctuated by two intervals (ca. 3–5 and ca. 13–16 ka cal BP) with a slight increase (average ca. 8 %–10 %) (Fig. 3). The median size was small during ca. 15–27.5 ka cal BP (ca. 235–456 cm) and ca. 0–2 ka cal BP (ca. 0–26 cm). In the period of 2–15 ka cal BP, the median size was relatively big, but at around 11 ka cal BP it is as small as that in other periods (Fig. 3).

TOC within the samples varies between 0.75 % and 15.13 %, and TN varies from 0.08 % to 2.01 % (Fig. 3). TOC increases from 9 % to 15 % between 27.5–20 ka cal BP and then decreases to 5 % around 12–9 ka cal BP. A sudden increase in TOC to 10 %–14 % occurs after 9 ka cal BP and then decreases sharply to 0.75 % between 5–3 ka cal BP before increasing again (Fig. 3). Variations in TN and TOC are highly synchronous (Fig. 3). The C/N ratio is around 10 during 27.5–13 ka cal BP and higher than 10 during 8–7 and 5–3 ka cal BP, with lower than 10 during 13–8, 7–5 and 3–0 ka cal BP (Fig. 3). The Fe / Mn ratio peaks around 13–9 ka cal BP (Fig. 3).

XRD detects quartz, calcite, aragonite, magnetite, muscovite, gypsum, rhodochrosite, dolomite and clinochlore as major minerals in the core sediments. Carbonate in the core appears primarily in two sections, between 0–180 and 226–288 cm (Fig. 3). Aragonite exists only in the upper 34 cm of sediments, which partially compensates for the decrease in calcite (Fig. 3). The $\delta^{18}O_{carb}$ varies from −8.435 ‰ to −2.525 ‰ during 18 to 14.5 ka cal BP and from −10.472 ‰ to −4.371 ‰ during 8.5–0.77 ka cal BP (Fig. 3). $^{18}O_{carb}$ enriched consistently since 8.5 ka cal BP (Fig. 3).

3.2 Pollen assemblage variations and reconstructed SWSI over the past 27 000 years

A total of 99 pollen taxa were identified in 114 samples. Pollen from tree taxa, including *Pinus*, *Picea*, evergreen and deciduous *Quercus* (*Quercus*.Eve and *Quercus*.Dec), *Betula* and *Tsuga*, dominated the entire pollen record, with an average percentage of 85.6 % (Fig. 4). The shrub taxa only accounts for 1.08 % of the entire pollen record. The average percentage of the herbaceous taxa is 13.3 %. Among the herb taxa, only *Artemisia*, Poaceae and Asteraceae have average percentages > 1 %. Herbs increased abruptly for several brief time intervals between 8–6 ka cal BP and between 3–2 ka cal BP (Fig. 4). The most noticeable change in the tree pollen composition occurred around 13 ka cal BP, when *Quercus*.Dec was replaced rapidly by *Quercus*.Eve and *Betula*, and the coniferous taxa (*Abies*, *Picea*, *Pinus* and *Tsuga*) almost disappeared (Fig. 4). Another obvious change in the pollen composition occurred at 3 ka cal BP, when *Pinus*, *Artemisia* and Poaceae increased considerably, and *Quercus*.Eve, *Quercus*.Dec, *Betula* and *Alnus* decreased. The average percentage of herbs was relatively low compared with woody plants throughout the core. But the abundance of herbaceous pollen increased noticeably between 8−6 ka cal BP and especially after 3 ka cal BP, with the maximum percentage more than 90 %.

A two-component WA-PLS model was selected on the basis of high r^2 (0.62), low RMSEP (0.159) and the smallest number of "useful" components (Table S1 in the Supplement). High (low) SWSI values indicate large (small)

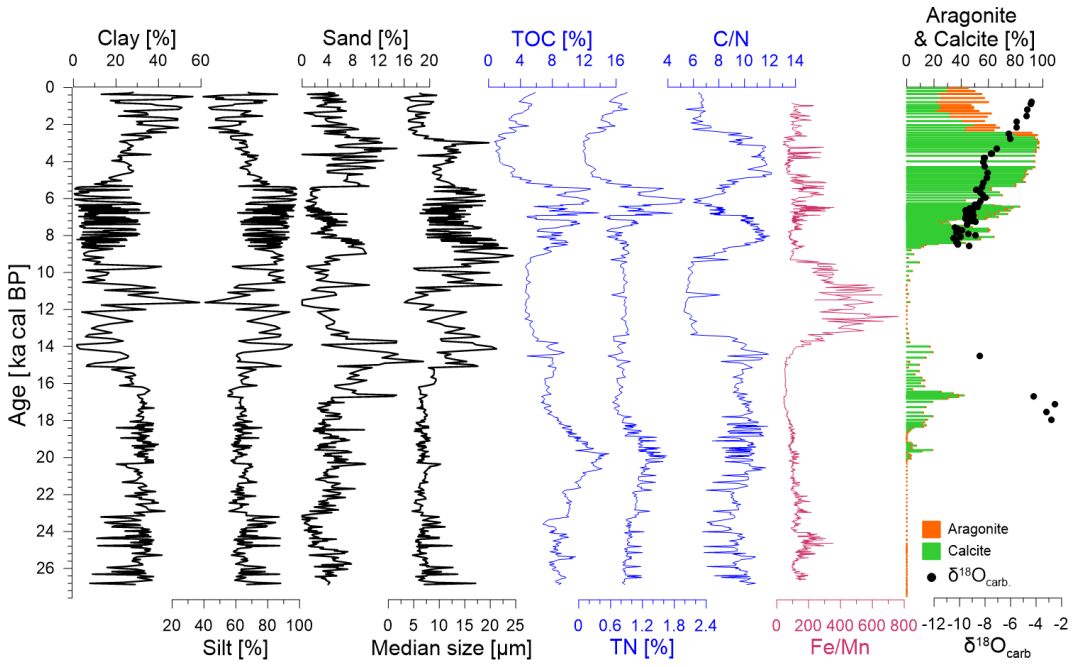

Figure 3. Down-core variations in the grain-size components (clay, silt and sand), median grain size, TOC and TN content, C/N and Fe/Mn ratios, calcite and aragonite content, and $\delta^{18}O_{carb}$.

amounts of water stress in soil system. The reconstructed SWSI ranges from 0–0.29, reflecting low to moderate water stress over the past 27 000 years. Relatively high SWSI occurred in three periods: 20–15 ka cal BP, 8–6 and 4–0 ka cal BP (Fig. 4).

4 Discussion

4.1 Precipitation change revealed by grain size

The grain size composition of lake sediments contains information on the sources of clastic materials, lake level fluctuations and transport energy related to variations in runoff (Peng et al., 2005; Xiao et al., 2013). A previous study on the spatial characteristics of grain-size distributions in the surface sediments of Yilong Lake revealed that, as the water depth decreased, the median size increased and the grain-size distribution curve changed from "unimodal" to "bimodal" (L. Zhang et al., 2019). Yilong Lake is located in the realm of the ISM, where the source of clastic materials (especially coarse particles) and the transport energy are primarily controlled by precipitation. An increase in precipitation not only enhances the erosion intensity of the basin, but also increases the runoff, which will lead to the transportation of more coarse particles into the lake. In the core YLH, most of the samples with a relatively large median grain size show a "unimodal" distribution (Fig. S2 in the Supplement), which implies a relatively high lake level and an increase in precipitation-transported coarse particles into the central part of the lake. Consequently, an increase in the sand component and median grain size coarsening should relate to intensified hydrological energy under increased precipitation.

Carbonate deposited from the lake water was assumed to preserve the $\delta^{18}O$ signal of precipitation, and hence the $\delta^{18}O_{carb}$ from lake sediments is a good proxy for reflecting precipitation intensity or ISM in the Yunnan region (Hillman et al., 2017, 2020; Hodell et al., 1999; Sun et al., 2019). A moderately strong negative correlation between precipitation $\delta^{18}O$ and monthly precipitation amount at Kunming, SW China, has been reported (Hillman et al., 2017). Therefore, the assumption that the $\delta^{18}O$ of the water in Yilong Lake was controlled by the $\delta^{18}O$ of precipitation is reasonable. The changes in the median grain size in core YHL closely match that of $\delta^{18}O_{carb}$, with the small grain size corresponding to high $\delta^{18}O_{carb}$ values, and vice versa (Fig. 5). This supports the theory that the median grain size is a reliable indicator of precipitation intensity in Yilong Lake. However, it should be noted that grain-size data from the samples in the last 3000 years cannot be simply interpreted as changes in precipitation intensity because human activities strongly affected the regional landscape and freshwater systems during this period (Wu et al., 2015; Xiao et al., 2017).

Variations of the median grain size from core YLH reflect less monsoonal precipitation during ca. 27–15 ka cal BP and generally high precipitation between ca. 15–3 ka cal BP (Fig. 5). This pattern is generally consistent with many lines of evidence from stalagmites (Cai et al., 2015; Cheng et al., 2016; Dykoski et al., 2005; Zhao et al., 2015) and lake sediments (Hodell et al., 1999; Peng et al., 2019; Sun et

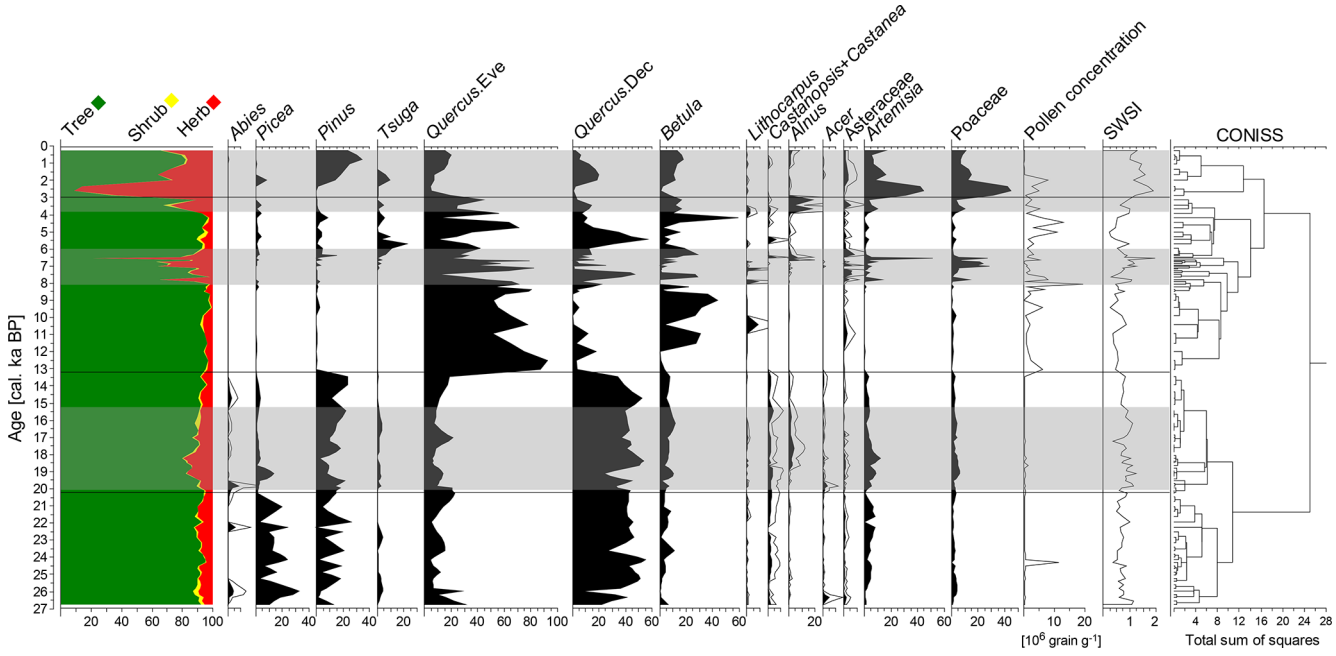

Figure 4. Pollen percentages diagram of the main taxa (average percentages ≥ 5 %), the pollen concentration and the reconstructed soil water stress index (SWSI). Pollen types with relatively low percentages have been magnified 3 times. Grey shadows mark periods of relatively high SWSI.

al., 2019). Additionally, variations of the median grain size also record the well-known climatic events Bølling–Allerød (B/A) and Younger Dryas (YD), shown respectively as a sharp increase and decrease in the monsoonal precipitation (Fig. 4). The occurrence time of the B/A event recorded in this study is consistent with that documented in the stalagmite δ^{18}O records from Cave Dongge (Dykoski et al., 2005), Sanbao (Cheng et al., 2016) and Xiaobailong (Cai et al., 2015) (Fig. 5). However, the YD event in this study lagged ca. 1000 years behind that recorded in the stalagmite δ^{18}O from Cave Dongge (Dykoski et al., 2005) and Sanbao (Cheng et al., 2016). This delayed monsoon signal is recorded in the stalagmite δ^{18}O record from Xiaobailong Cave (Cai et al., 2015) which is only ca. 85 km away from Yilong Lake. Understanding the mechanisms driving this lag is beyond the scope of this study, but uneven rainfall distribution due to the complex topography of the Yunnan-Guizhou Plateau likely played an important role.

4.2 Carbonate deposition as a record of past hydrological balance

Carbonate deposition in Yilong Lake is mainly composed of autochthonous calcite and aragonite (Fig. S3 in the Supplement). A large number of mollusc shells are the main source of the aragonite that only appears in the upper 34 cm of the core. Autochthonous calcite precipitation needs a certain degree of supersaturation (Raidt and Koschel, 1988) which can be achieved by seasonal temperature increases and plankton flourishing (Robbins and Blackwelder, 1992; Stabel, 1986). ^{18}O measurements of the lake water and precipitation indicated significant evaporative effects in Yilong Basin during the warm season (Whitmore et al., 1997). Increased temperature exerts a direct control on water evaporation, which will concentrate dissolved carbonates and hence facilitate carbonate precipitation. Photosynthesis of plankton influences carbonate precipitation by affecting CO_2 and pH in the epilimnetic water and/or providing nucleation sites for crystallisation (Robbins and Blackwelder, 1992; Stabel, 1986). Assuming that lake primary productivity played a big role in carbonate precipitation, algae productivity should have increased during 20–14 ka cal BP when carbonate content increased, and decreased during 14–9 ka cal BP when carbonate content decreased. But in fact, relatively high C/N values between 20–14 ka cal BP and low values between 14–9 ka cal BP indicate relatively low and high algae productivity, respectively. In addition, characteristics of the crystal morphology of calcite also indicate abiotic origins (Fig. S3 in the Supplement). Consequently, lake primary productivity is not a main cause for carbonates precipitated in Yilong Lake. The carbonate content in the lake sediments should reflect the hydrological balance (i.e. $P–E$).

The variations of the carbonate content in the lake sediments (Fig. 3) indicate a relatively positive water balance between 27–20 and 14–9 ka cal BP, and a negative water balance between 20–14 and 9–0 ka cal BP. Carbonate records from the two nearby shallow lakes Xingyun and Qilu (Fig. 1, Hillman et al., 2017, 2020; Hodell et al., 1999) show broadly

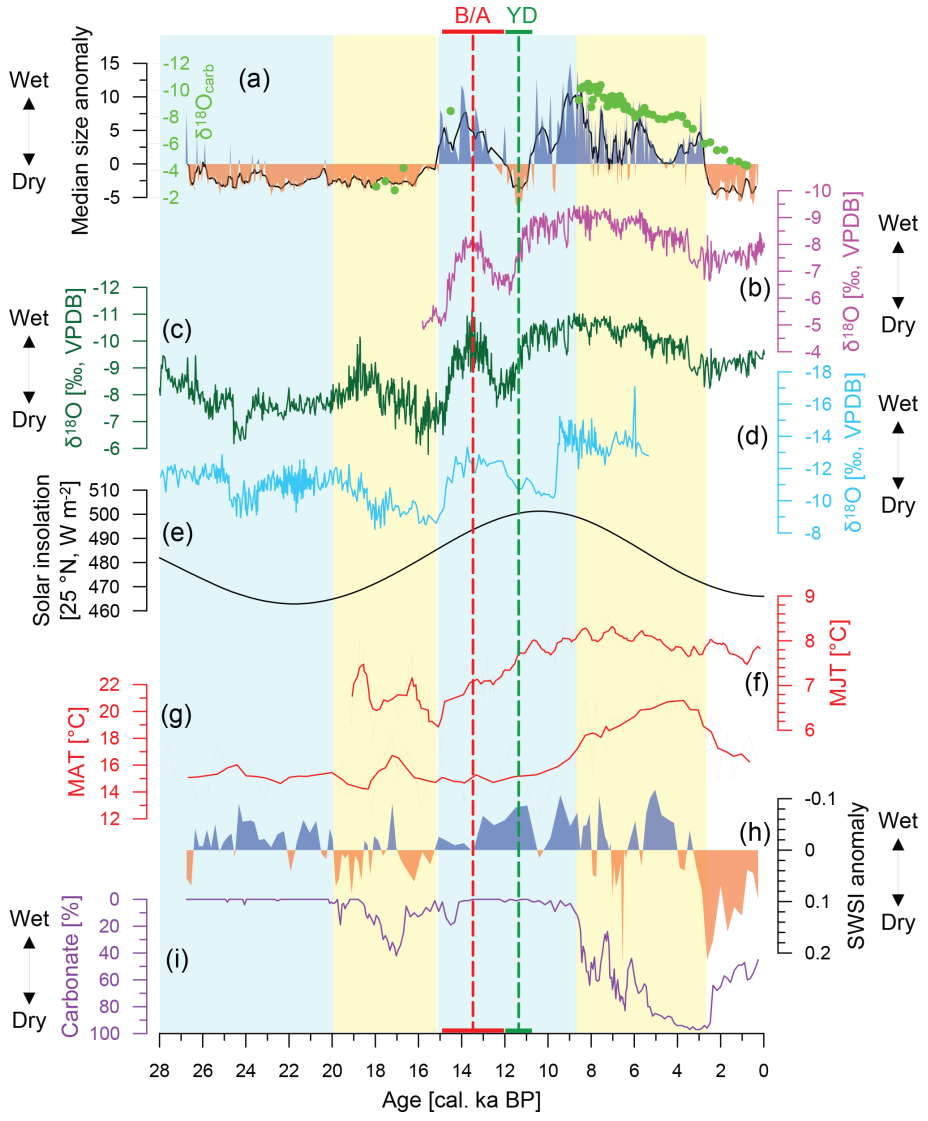

Figure 5. Median size and $\delta^{18}O_{carb}$ values from Yilong Lake **(a)**; stalagmite $\delta^{18}O$ records from Sanbao Cave (Cheng et al., 2016) **(b)**, Dongge Cave (Dykoski et al., 2005) **(c)** and Xiaobailong Cave (Cai et al., 2015) **(d)**; summer insolation curve for 25° N **(e)**; chironomid-mean July temperature (MJT) from Tiancai Lake (E. Zhang et al., 2019) **(f)**; brGDGT-derived mean annual temperature (MAT) from Qionghai Lake (Wang et al., 2020) **(g)**; pollen-based reconstructed soil water stress index (SWSI) for Yilong region **(h)**; carbonate content of sediments from Yilong Lake **(i)**. Light yellow (blue) shadows denote periods of inconsistency (consistency) of dry–wet conditions among precipitation, SWSI and hydrological balance.

similar patterns to this record, indicating that the hydrological changes reconstructed in this study reflect a regional rather than a local climate signal.

4.3 Different patterns of long-term changes in precipitation, hydrological balance and SWSI, and the potential mechanisms

Precipitation is the primary source of water for lacustrine systems and soils. It is generally assumed that dry conditions occurred when precipitation was low, and wet conditions prevailed when precipitation was high. From this point of view, we may conclude that our study region experienced "dry" conditions during the cold LGM and a "wet" phase during the warm Holocene. This pattern generally agrees with other paleoclimate reconstructions from the Yunnan region (e.g. Cheng et al., 2016; Xiao et al., 2014b). However, it does not match well with the hydrological balance and SWSI reconstructions from the same core. This study finds that during the LGM (27–20 ka cal BP) and the YD event, precipitation was low but the water balance of Yilong Lake was positive and the soil moisture was relatively high. During the early to late Holocene (9–3 ka cal BP), precipitation was high but the water balance was negative. The definition of dryness is the

shortage of available water, which is fundamentally a trade-off between water input and output (Breshears et al., 2005; Dai et al., 2018; Mishra and Singh, 2010; Trenberth et al., 2014; Watras et al., 2014). Therefore, factors controlling water loss from terrestrial systems can also play a large role in the creation of dry conditions.

Evaporation is one of the important pathways by which water is lost from terrestrial environments. The evaporation rate is higher at higher temperatures because the average kinetic energy of the water molecules increases and more can fly off the surface. Our pollen record revealed that *Quercus*.Dec and the coniferous taxa were rapidly replaced by *Quercus*.Eve and *Betula* around 13 ka cal BP (Fig. 3). According to the Vegetation Map of the People's Republic of China (The Editorial Committee of Vegetation Map of China, CAS, 2007), deciduous broad-leaved forest is distributed in areas with lower temperature compared to evergreen broad-leaved forest. Therefore, the characteristics of the pollen compositional change during the transition from glacial to post-glacial period reflects rising temperature. The LGM was characterised by low temperatures under which the simulated annual-mean potential evapotranspiration decreased by 10 %–40 % over nearly all land (Scheff et al., 2017). Decreasing evaporation is a major driver of increasing effective summer moisture availability, which has a profound influence on the hydrological states of lakes (Aichner et al., 2019). These factors can explain the positive hydrological balance and relatively wet soils reconstructed during the LGM. The precipitation during 20–15 ka cal BP was as low as the previous period while insolation was increasing (Fig. 5). Our pollen record showed an obvious decrease in *Picea*, indicating a warmer climate during 20–15 ka cal BP than in the previous period. This period corresponds to the late glacial warming which is widely reported in the Yunnan region (Fig. 5, Wang et al., 2020; Xiao et al., 2014b; E. Zhang et al., 2019). The increased temperature would intensify evaporation and lead to water deficiency in lacustrine and soil environments. Therefore, the hydrological and soil drying during 20–15 ka cal BP should be triggered by increasing temperatures. However, in spite of the high temperatures, soil moisture was still relatively high during 9–3 ka cal BP (Fig. 5). Water loss from soil systems is more complex than that from free water surfaces because both temperature and the underlying surface conditions affect the ways and the amount of soil water loss or soil water storage capacity (Maxwell and Condon, 2016; Zhang and Schilling, 2006).

Water is distributed across the landscape during a rainfall event, with precipitation intercepted by foliage, stored in the soil profile or collected in groundwater aquifers. The amount of water stored in soil profiles and aquifers can be regulated by plant processes (Guzha et al., 2018; Mohammad and Adam, 2010). Previous studies have shown that, both at a stand level and at a global scale, plant transpiration accounts for the largest portion of the total evapotranspiration (61 % ± 15 % SD–64 % ± 13 % SD, Good et al., 2015; Maxwell and Condon, 2016; Schlesinger and Jasechko, 2014). Our results show that the pollen concentration was high during 9–3 ka cal BP. Although there is not an obvious linear correlation between pollen concentration and vegetation cover (Luo et al., 2009; Xu et al., 2007), a three-fold increase in the average pollen concentration from the late Pleistocene to Holocene period can be interpreted as a relatively large change in the plant biomass through time. An increase in aboveground biomass likely increased the vegetation canopy and root biomass density (Cairns et al., 1997), causing more water loss from deeper soil layers and aquifers by transpiration through leave stomata, rather than evaporative loss directly from shallow soil (Lawrence and Slingo, 2004; Markewitz et al., 2010). The abundant precipitation and denser canopy cover in the early to middle Holocene resulted in a period of higher soil moisture availability, despite increasing temperatures and plant biomass likely causing an increase in the total evapotranspiration at this time.

The results of this study show that over the last 3000 years the meteorological, hydrological and soil systems were all in a dry phase (Fig. 5). At the same time, human activities had intensified and changed the underlying surface conditions in the Yunnan region (Xiao et al., 2017, 2018). *Pinus* sp. are typically pioneer species, which can colonise disturbed sites if competition and grazing pressures are low. Increases in Poaceae pollen abundance is commonly interpreted as reflecting increased regional aridity, but it is also influenced by early farming activities. If climate change was the only critical cause for vegetation change during the last 3000 years, the vegetation composition should have changed to a status similar to that recorded in the previous "cool–dry" period. However, the results of the cluster analysis show that samples from the last 3000 years appear across all three clusters identifying the late glacial period, early Holocene and mid to late Holocene (Fig. S4 in the Supplement). Therefore, the pollen-based SWSI may have failed to reflect the real soil moisture conditions for the recent 3000 years. At present, we cannot estimate the impacts and effects of human activities on lake hydrologic regimes and watershed landscapes in this period. Thus, producing an accurate reconstruction of the monsoonal precipitation, hydrological balance and soil moisture for the past 3000 years is limited.

5 Conclusions

Sedimentological and pollen data from Yilong Lake provide a 27 000-year perspective of local and regional variations in the ISM precipitation, hydrological balance and soil moisture conditions in SW China. The results show that the reconstructed precipitation is generally consistent with the regional pattern, with low precipitation during the LGM and the YD event and high precipitation during the B/A event and the early to middle Holocene. But since the LGM, the long-term changes in precipitation, hydrological balance and

soil moisture are not completely consistent. On a millennial scale, the hydrological balance was more sensitive to temperature change, which directly controls the lake surface evaporation rate. In addition to precipitation and temperature, plant processes may also play a large role in regulating soil moisture. Plant biomass in the Yilong area increased during the early to middle Holocene as recorded in the pollen records. This likely increased the vegetation canopy, causing less water loss from shallow soil via evaporation. Human activities intensified during the last 3000 years. It is difficult to estimate the impact of human activities on the regional landscape and on the watershed hydrology in SW China in the late Holocene. Therefore, the reconstructed deficit in the hydrological and soil systems during this period cannot be interpreted simply as climate change. Finally, our study highlights that "wetness" and "dryness" should be precisely defined when interpreting different paleoproxies.

Data availability. The reconstructed data presented in the paper can be accessed by contacting Mengna Liao or Jian Ni.

Supplement. The supplement related to this article is available online at: https://doi.org/10.5194/cp-17-2291-2021-supplement.

Author contributions. ML, KL and JN developed the research questions. ML, KL and WS designed and conducted the experiment. KL conducted the fieldwork. ML, KL and WS analysed samples and processed data. ML and KL wrote the paper with contributions from all co-authors.

Competing interests. The contact author has declared that neither they nor their co-authors have any competing interests.

Disclaimer. Publisher's note: Copernicus Publications remains neutral with regard to jurisdictional claims in published maps and institutional affiliations.

Acknowledgements. We appreciated Hongbo Zheng and Zhujun Hu from Nanjing Normal University for their help with the XRF core scanning, Shijie Li from the Institute of Geochemistry at CAS for field sampling, and Lydia Lattin Mackenzie from Zhejiang University for language editing.

Financial support. This research has been supported by the Strategic Priority Research Program of the Chinese Academy of Sciences (grant nos. XDA2009000003, XDB40000000), the Nanjing Institute of Geography and Limnology of the Chinese Academy of Sciences (grant no. 2021NIGLAS-CJH03), and the National Basic Research Program of China (grant no. 2016YFC0502101).

Review statement. This paper was edited by Julie Loisel and reviewed by Vera Markgraf and one anonymous referee.

References

Ahn, J., Wahlen, M., Deck, B. L., Brook, E. J., Mayewski, P. A., Taylor, K. C., and White, J. W.: A record of atmospheric CO_2 during the last 40 000 years from the Siple Dome, Antarctica ice core, J. Geophys. Res.-Atmos., 109, D13305, https://doi.org/10.1029/2003JD004415, 2004.

Aichner, B., Makhmudov, Z., Rajabov, I., Zhang, Q., Pausata, F. S., Werner, M., Heinecke, L., Kuessner, M. L., Feakins, S. J., and Sachse, D.: Hydroclimate in the Pamirs was driven by changes in precipitation-evaporation seasonality since the Last Glacial Period, Geophys. Res. Lett., 46, 13972–13983, https://doi.org/10.1029/2019GL085202, 2019.

Blaauw, M., Christen, J. A., and Lopez, M. A. A.: rbacon: Age-depth modelling using Bayesian statistics, R package version 2.5.0 [code], available at: https://CRAN.R-project.org/package=rbacon, last access date: 15 November 2020.

Breshears, D. D., Cobb, N. S., Rich, P. M., Price, K. P., Allen, C. D., Balice, R. G., Romme, W. H., Kastens, J. H., Floyd, M. L., and Belnap, J.: Regional vegetation die-off in response to global-change-type drought, P. Natl. Acad. Sci. USA, 102, 15144–15148, https://doi.org/10.1073/pnas.0505734102, 2005.

Cai, Y., Fung, I. Y., Edwards, R. L., An, Z., Cheng, H., Lee, J.-E., Tan, L., Shen, C.-C., Wang, X., and Day, J. A.: Variability of stalagmite-inferred Indian monsoon precipitation over the past 252 000 yrs, P. Natl. Acad. Sci. USA, 112, 2954–2959, https://doi.org/10.1073/pnas.1424035112, 2015.

Cairns, M. A., Brown, S., Helmer, E. H., and Baumgardner, G. A.: Root biomass allocation in the world's upland forests, Oecologia, 111, 1–11, https://doi.org/10.1007/s004420050201, 1997.

Chen, X., Chen, F., Zhou, A., Huang, X., Tang, L., Wu, D., Zhang, X., and Yu, J.: Vegetation history, climatic changes and Indian summer monsoon evolution during the Last Glaciation (36,400–13,400 cal yr BP) documented by sediments from Xingyun Lake, Yunnan, China, Palaeogeogr. Palaeocl., 410, 179–189, https://doi.org/10.1016/j.palaeo.2014.05.027, 2014.

Cheng, H., Edwards, R. L., Sinha, A., Spötl, C., Yi, L., Chen, S., Kelly, M., Kathayat, G., Wang, X., and Li, X.: The Asian monsoon over the past 640,000 years and ice age terminations, Nature, 534, 640–646, https://doi.org/10.1038/nature18591, 2016.

Cook, C. G., Jones, R. T., Langdon, P. G., Leng, M. J., and Zhang, E.: New insights on Late Quaternary Asian palaeomonsoon variability and the timing of the Last Glacial Maximum in southwestern China, Quaternary Sci. Rev., 30, 808–820, https://doi.org/10.1016/j.quascirev.2011.01.003, 2011.

Dai, A., Zhao, T., and Chen, J.: Climate change and drought: A precipitation and evaporation perspective, Curr. Clim. Change Rep., 4, 301–312, https://doi.org/10.1007/s40641-018-0101-6, 2018.

Davis, T. W., Prentice, I. C., Stocker, B. D., Thomas, R. T., Whitley, R. J., Wang, H., Evans, B. J., Gallego-Sala, A. V., Sykes, M. T., and Cramer, W.: Simple process-led algorithms for simulating habitats (SPLASH v.1.0): robust indices of radiation, evapotranspiration and plant-available moisture, Geosci. Model Dev., 10, 689–708, https://doi.org/10.5194/gmd-10-689-2017, 2017.

Dykoski, C. A., Edwards, R. L., Cheng, H., Yuan, D., Cai, Y., Zhang, M., Lin, Y., Qing, J., An, Z., and Revenaugh, J.: A high-

resolution, absolute-dated Holocene and deglacial Asian monsoon record from Dongge Cave, China, Earth Planet. Sc. Lett., 233, 71–86, https://doi.org/10.1016/j.epsl.2005.01.036, 2005.

Faegri, K., Kaland, P. E., and Krzywinski, K. (Eds.): Textbook of pollen analysis, 4th edn. John Wiley and Sons Ltd., Chichester, United Kingdom, ISBN: 0 471 92178 5, 1989.

Farr, T. G., Rosen, P. A., Caro, E., Crippen, R., Duren, R., Hensley, S., Kobrick, M., Paller, M., Rodriguez, E., Roth, L., Seal, D., Shaffer, S., Shimada, J., Umland, J., Werner, M., Oskin, M., Burbank, D., and Alsdorf, D.: The shuttle radar topography mission, Rev. Geophys., 45, RG2004, https://doi.org/10.1029/2005RG000183, 2007.

Feng, H. and Liu, Y.: Combined effects of precipitation and air temperature on soil moisture in different land covers in a humid basin, J. Hydrol., 531, 1129–1140, https://doi.org/10.1016/j.jhydrol.2015.11.016, 2015.

Good, S. P., Noone, D., and Bowen, G.: Hydrologic connectivity constrains partitioning of global terrestrial water fluxes, Science, 349, 175–177, https://doi.org/10.1126/science.aaa5931, 2015.

Guzha, A., Rufino, M. C., Okoth, S., Jacobs, S., and Nóbrega, R.: Impacts of land use and land cover change on surface runoff, discharge and low flows: Evidence from East Africa, J. Hydrol.-Reg. Stud., 15, 49–67, https://doi.org/10.1016/j.ejrh.2017.11.005, 2018.

Hancock, P. A. and Hutchinson, M.: Spatial interpolation of large climate data sets using bivariate thin plate smoothing splines, Environ. Modell. Softw., 21, 1684–1694, https://doi.org/10.1016/j.envsoft.2005.08.005, 2006.

Hillman, A. L., Abbott, M. B., Finkenbinder, M. S., and Yu, J.: An 8,600 year lacustrine record of summer monsoon variability from Yunnan, China, Quaternary Sci. Rev., 174, 120–132, https://doi.org/10.1016/j.quascirev.2017.09.005, 2017.

Hillman, A. L., O'Quinn, R. F., Abbott, M. B., and Bain, D. J.: A Holocene history of the Indian monsoon from Qilu Lake, southwestern China, Quaternary Sci. Rev., 227, 106051, https://doi.org/10.1016/j.quascirev.2019.106051, 2020.

Hodell, D. A., Brenner, M., Kanfoush, S. L., Curtis, J. H., Stoner, J. S., Xueliang, S., Yuan, W., and Whitmore, T. J.: Paleoclimate of southwestern China for the past 50 000 yr inferred from lake sediment records, Quaternary Res., 52, 369–380, https://doi.org/10.1006/qres.1999.2072, 1999.

Huang, C., Wei, G., Ma, J., and Liu, Y.: Evolution of the Indian summer monsoon during the interval 32.7–11.4 cal. ka BP: Evidence from the Baoxiu peat, Yunnan, southwest China, J. Asian Earth Sci., 131, 72–80, https://doi.org/10.1016/j.jseaes.2016.09.008, 2016.

Hutchinson, M. (Ed.): ANUSPLIN version 4.36 user guide, Centre for Resource and Environmental Studies, the Australian National University, Canberra, Australia, 54 pp. ISBN: 086740 512 0, 2006.

Juggins, S.: rioja: Analysis of Quaternary Science Data, R package version (0.9-15.1) [code], available at: http://cran.r-project.org/package=rioja Last access date: 26 October 2020, 2017.

Lawrence, D. M. and Slingo, J. M.: An annual cycle of vegetation in a GCM. Part I: implementation and impact on evaporation, Clim. Dynam., 22, 87–105, https://doi.org/10.1007/s00382-003-0366-9, 2004.

Leng, M. J. and Marshall, J. D.: Palaeoclimate interpretation of stable isotope data from lake sediment archives, Quaternary Sci. Rev., 23, 811–831, https://doi.org/10.1016/j.quascirev.2003.06.012, 2004.

Li, Y., Chen, X., Xiao, X., Zhang, H., Xue, B., Shen, J., and Zhang, E.: Diatom-based inference of Asian monsoon precipitation from a volcanic lake in southwest China for the last 18.5 ka, Quaternary Sci. Rev., 182, 109–120, https://doi.org/10.1016/j.quascirev.2017.11.021, 2018.

Luo, C., Zheng, Z., Tarasov, P., Pan, A., Huang, K., Beaudouin, C., and An, F.: Characteristics of the modern pollen distribution and their relationship to vegetation in the Xinjiang region, northwestern China, Rev. Palaeobot. Palyno., 153, 282–295, https://doi.org/10.1016/j.revpalbo.2008.08.007, 2009.

Markewitz, D., Devine, S., Davidson, E. A., Brando, P., and Nepstad, D. C.: Soil moisture depletion under simulated drought in the Amazon: impacts on deep root uptake, New Phytol., 187, 592–607, https://doi.org/10.1111/j.1469-8137.2010.03391.x, 2010.

Maxwell, R. M. and Condon, L. E.: Connections between groundwater flow and transpiration partitioning, Science, 353, 377–380, https://doi.org/10.1126/science.aaf7891, 2016.

Mishra, A. K. and Singh, V. P.: A review of drought concepts, J. Hydrol., 391, 202–216, https://doi.org/10.1016/j.jhydrol.2010.07.012, 2010.

Mohammad, A. G. and Adam, M. A.: The impact of vegetative cover type on runoff and soil erosion under different land uses, Catena, 81, 97–103, https://doi.org/10.1016/j.catena.2010.01.008, 2010.

Ni, J., Cao, X., Jeltsch, F., and Herzschuh, U.: Biome distribution over the last 22,000 yr in China, Palaeogeogra. Palaeocl., 409, 33–47, https://doi.org/10.1016/j.palaeo.2014.04.023, 2014.

Ning, D., Zhang, E., Sun, W., Chang, J., and Shulmeister, J.: Holocene Indian Summer Monsoon variation inferred from geochemical and grain size records from Lake Ximenglongtan, southwestern China, Palaeogeogra. Palaeocl., 487, 260–269, https://doi.org/10.1016/j.palaeo.2017.09.008, 2017.

Ohlendorf, C., Fey, M., Gebhardt, C., Haberzettl, T., Lücke, A., Mayr, C., Schäbitz, F., Wille, M., and Zolitschka, B.: Mechanisms of lake-level change at Laguna Potrok Aike (Argentina) – insights from hydrological balance calculations, Quaternary Sci. Rev., 71, 27–45, https://doi.org/10.1016/j.quascirev.2012.10.040, 2013.

Peng, J., Yang, X., Toney, J. L., Ruan, J., Li, G., Zhou, Q., Gao, H., Xie, Y., Chen, Q., and Zhang, T.: Indian Summer Monsoon variations and competing influences between hemispheres since ∼35 ka recorded in Tengchongqinghai Lake, southwestern China, Palaeogeogra. Palaeocl., 516, 113–125, https://doi.org/10.1016/j.palaeo.2018.11.040, 2019.

Peng, Y., Xiao, J., Nakamura, T., Liu, B., and Inouchi, Y.: Holocene East Asian monsoonal precipitation pattern revealed by grain-size distribution of core sediments of Daihai Lake in Inner Mongolia of north-central China, Earth Planet. Sc. Lett., 233, 467–479, https://doi.org/10.1016/j.epsl.2005.02.022, 2005.

Pokhrel, Y., Felfelani, F., Satoh, Y., Boulange, J., Burek, P., Gädeke, A., Gerten, D., Gosling, S. N., Grillakis, M., and Gudmundsson, L.: Global terrestrial water storage and drought severity under climate change, Nat. Clim. Change, 11, 226–233, https://doi.org/10.1038/s41558-020-00972-w, 2021.

Prentice, I. C.: Multidimensional scaling as a research tool in Quaternary palynology: a review of theory and methods, Rev.

Palaeobot. Palyno., 31, 71–104, https://doi.org/10.1016/0034-6667(80)90023-8, 1980.

Prentice, I. C., Sykes, M. T., and Cramer, W.: A simulation model for the transient effects of climate change on forest landscapes, Ecol. Model., 65, 51–70, https://doi.org/10.1016/0304-3800(93)90126-D, 1993.

Qiu, J.: China drought highlights future climate threats: Yunnan's worst drought for many years has been exacerbated by destruction of forest cover and a history of poor water management, Nature, 465, 142–144, https://doi.org/10.1038/465142a, 2010.

Raidt, H. and Koschel, R.: Morphology of calcite crystals in hardwater lakes, Limnologica, 19, 3–12, 1988.

R Core Team: R: A language and environment for statistical computing, R Foundation for Statistical Computing [code], available at: https://www.R-project.org/ (last access: 15 November 2020), 2018.

Reimer, P. J., Austin, W. E. N., Bard, E., Bayliss, A., Blackwell, P. G., Ramsey, C. B., Butzin, M., Cheng, H., Edwards, R. L., Friedrich, M., Grootes, P. M., Guilderson, T. P., Hajdas, I., Heaton, T. J., Hogg, A. G., Hughen, K. A., Kromer, B., Manning, S. W., Muscheler, R., Palmer, J. G., Pearson, C., van der Plicht, J., Reimer, R. W., Richards, D. A., Scott, E. M., Southon, J. R., Turney, C. S. M., Wacker, L., Adolphi, F., Büntgen, U., Capano, M., Fahrni, S. M., Fogtmann-Schulz, A., Friedrich, R., Köhler, P., Kudsk, S., Miyake, F., Olsen, J., Reinig, F., Sakamoto, M., Sookdeo, A., and Talamo, S.: The IntCal20 Northern Hemisphere radiocarbon age calibration curve (0–55 cal. ka BP), Radiocarbon, 62, 725–757, https://doi.org/10.1017/RDC.2020.41, 2020.

Robbins, L. and Blackwelder, P.: Biochemical and ultrastructural evidence for the origin of whitings: A biologically induced calcium carbonate precipitation mechanism, Geology, 20, 464–468, https://doi.org/10.1130/0091-7613(1992)020<0464:BAUEFT>2.3.CO;2, 1992.

Scheff, J., Seager, R., Liu, H., and Coats, S.: Are glacials dry? Consequences for paleoclimatology and for greenhouse warming, J. Climate, 30, 6593–6609, https://doi.org/10.1175/JCLI-D-16-0854.1, 2017.

Schlesinger, W. H. and Jasechko, S.: Transpiration in the global water cycle, Agr. Forest Meteorol., 189, 115–117, https://doi.org/10.1016/j.agrformet.2014.01.011, 2014.

Sheng, E., Yu, K., Xu, H., Lan, J., Liu, B., and Che, S.: Late holocene Indian summer monsoon precipitation history at Lake Lugu, northwestern Yunnan Province, southwestern China, Palaeogeogra. Palaeocl., 438, 24–33, https://doi.org/10.1016/j.palaeo.2015.07.026, 2015.

Stabel, H.-H.: Calcite precipitation in Lake Constance: Chemical equilibrium, sedimentation, and nucleation by algae, Limnol. Oceanogr., 31, 1081–1093, https://doi.org/10.4319/lo.1986.31.5.1081, 1986.

Sun, S., Chen, H., Ju, W., Wang, G., Sun, G., Huang, J., Ma, H., Gao, C., Hua, W., and Yan, G.: On the coupling between precipitation and potential evapotranspiration: contributions to decadal drought anomalies in the Southwest China, Clim. Dynam., 48, 3779–3797, https://doi.org/10.1007/s00382-016-3302-5, 2017.

Sun, W., Zhang, E., Shulmeister, J., Bird, M. I., Chang, J., and Shen, J.: Abrupt changes in Indian summer monsoon strength during the last deglaciation and early Holocene based on stable isotope evidence from Lake Chenghai, southwest China, Quaternary Sci. Rev., 218, 1–9, https://doi.org/10.1016/j.quascirev.2019.06.006, 2019.

ter Braak, C. J. and Juggins, S.: Weighted averaging partial least squares regression (WA-PLS): an improved method for reconstructing environmental variables from species assemblages, Twelfth international diatom symposium, Renesse, the Netherlands, 30 August–5 September 1992, 485–502, https://doi.org/10.1007/BF00028046, 1993.

The Editorial Committee of Vegetation Map of China, Chinese Academy of Sciences (Ed.): Vegetation Map of the People's Republic of China (1 : 1 000 000), Geological Publishing House, Beijing, ISBN: 978-7-116-05146-1, 10–11, 2007.

Trenberth, K. E., Dai, A., Van Der Schrier, G., Jones, P. D., Barichivich, J., Briffa, K. R., and Sheffield, J.: Global warming and changes in drought, Nat. Clim. Change, 4, 17–22, https://doi.org/10.1038/nclimate2067, 2014.

Wang, G., Wang, Y., Wei, Z., He, W., Ma, X., Sun, Z., Xu, L., Gong, J., Wang, Z., and Pan, Y.: Paleoclimate changes of the past 30 cal ka BP inferred from lipid biomarkers and geochemical records from Qionghai Lake, southwest China, J. Asian Earth Sci., 172, 346–358, https://doi.org/10.1016/j.jseaes.2018.09.019, 2019.

Wang, G., Wang, Y., Wei, Z., He, W., Ma, X., and Zhang, T.: Reconstruction of temperature and precipitation spanning the past 28 000 yrs based on branched tetraether lipids from Qionghai Lake, southwestern China, Palaeogeogra. Palaeocl., 562, 110094, https://doi.org/10.1016/j.palaeo.2020.110094, 2020.

Wang, L., Yuan, X., Xie, Z., Wu, P., and Li, Y.: Increasing flash droughts over China during the recent global warming hiatus, Sci. Rep-UK, 6, 30571, https://doi.org/10.1038/srep30571, 2016.

Wang, S. and Dou, H. (Eds.): The lake inventory of China, Science Press, Beijing, 379–381, ISBN 7-203-006706-1, 1998.

Watras, C., Read, J., Holman, K., Liu, Z., Song, Y. Y., Watras, A., Morgan, S., and Stanley, E.: Decadal oscillation of lakes and aquifers in the upper Great Lakes region of North America: Hydroclimatic implications, Geophys. Res. Lett., 41, 456–462, https://doi.org/10.1002/2013GL058679, 2014.

Wei, G., Xie, L., Sun, Y., Lu, Y., and Liu, Y.: Major and trace elements of a peat core from Yunnan, Southwest China: implications for paleoclimatic proxies, J. Asian Earth Sci., 58, 64–77, https://doi.org/10.1016/j.jseaes.2012.06.021, 2012.

Whitmore, T. J., Brenner, M., Jiang, Z., Curtis, J. H., Moore, A., Engstrom, D. R., and Wu, Y.: Water quality and sediment geochemistry in lakes of Yunnan Province, southern China, Environ. Geol., 32, 45–55, https://doi.org/10.1007/s002540050192, 1997.

Wu, D., Zhou, A., Liu, J., Chen, X., Wei, H., Sun, H., Yu, J., Bloemendal, J., and Chen, F.: Changing intensity of human activity over the last 2,000 years recorded by the magnetic characteristics of sediments from Xingyun Lake, Yunnan, China, J. Paleolimnol., 53, 47–60, https://doi.org/10.1007/s10933-014-9806-2, 2015.

Wu, D., Chen, X., Lv, F., Brenner, M., Curtis, J., Zhou, A., Chen, J., Abbott, M., Yu, J., and Chen, F.: Decoupled early Holocene summer temperature and monsoon precipitation in southwest China, Quaternary Sci. Rev., 193, 54–67, https://doi.org/10.1016/j.quascirev.2018.05.038, 2018.

Xiao, J., Fan, J., Zhou, L., Zhai, D., Wen, R., and Qin, X.: A model for linking grain-size component to lake level status

of a modern clastic lake, J. Asian Earth Sci., 69, 149–158, https://doi.org/10.1016/j.jseaes.2012.07.003, 2013.

Xiao, X., Haberle, S. G., Yang, X., Shen, J., Han, Y., and Wang, S.: New evidence on deglacial climatic variability from an alpine lacustrine record in northwestern Yunnan Province, southwestern China, Palaeogeogr. Palaeocl., 406, 9–21, https://doi.org/10.1016/j.palaeo.2014.04.008, 2014a.

Xiao, X., Haberle, S. G., Shen, J., Yang, X., Han, Y., Zhang, E., and Wang, S.: Latest Pleistocene and Holocene vegetation and climate history inferred from an alpine lacustrine record, northwestern Yunnan Province, southwestern China, Quaternary Sci. Rev., 86, 35–48, https://doi.org/10.1016/j.quascirev.2013.12.023, 2014b.

Xiao, X., Haberle, S. G., Shen, J., Xue, B., Burrows, M., and Wang, S.: Postglacial fire history and interactions with vegetation and climate in southwestern Yunnan Province of China, Clim. Past, 13, 613–627, https://doi.org/10.5194/cp-13-613-2017, 2017.

Xiao, X., Haberle, S. G., Li, Y., Liu, E., Shen, J., Zhang, E., Yin, J., and Wang, S.: Evidence of Holocene climatic change and human impact in northwestern Yunnan Province: High-resolution pollen and charcoal records from Chenghai Lake, southwestern China, Holocene, 28, 127–139, https://doi.org/10.1177/0959683617715692, 2018.

Xu, H., Lan, J., Zhang, G., and Zhou, X.: Arid Central Asia saw mid-Holocene drought, Geology, 47, 255–258, https://doi.org/10.1130/G45686.1, 2019.

Xu, Q., Li, Y., Yang, X., and Zheng, Z.: Quantitative relationship between pollen and vegetation in northern China, Sci. China Ser. D, 50, 582–599, https://doi.org/10.1007/s11430-007-2044-y, 2007.

Zhang, E., Chang, J., Cao, Y., Sun, W., Shulmeister, J., Tang, H., Langdon, P. G., Yang, X., and Shen, J.: Holocene high-resolution quantitative summer temperature reconstruction based on subfossil chironomids from the southeast margin of the Qinghai-Tibetan Plateau, Quaternary Sci. Rev., 165, 1–12, https://doi.org/10.1016/j.quascirev.2017.04.008, 2017.

Zhang, E., Chang, J., Shulmeister, J., Langdon, P., Sun, W., Cao, Y., Yang, X., and Shen, J.: Summer temperature fluctuations in Southwestern China during the end of the LGM and the last deglaciation, Earth Planet. Sc. Lett., 509, 78–87, https://doi.org/10.1016/j.epsl.2018.12.024, 2019.

Zhang, L., Zhang, H., Chang, F., Duan, L., Hu, J., Li, T., Cai, M., and Zhang, Y.: Spatial variation characteristics of sediment size and its environmental indication significance in Lake Yilong, Yunnan Province, Quaternary Sci., 39, 1159–1170, https://doi.org/10.11928/j.issn.1001-7410.2019.05.08, 2019 (in Chinese with English abstract).

Zhang, Y.-K. and Schilling, K.: Effects of land cover on water table, soil moisture, evapotranspiration, and groundwater recharge: a field observation and analysis, J. Hydrol., 319, 328–338, https://doi.org/10.1016/j.jhydrol.2005.06.044, 2006.

Zhao, M., Li, H.-C., Liu, Z.-H., Mii, H.-S., Sun, H.-L., Shen, C.-C., and Kang, S.-C.: Changes in climate and vegetation of central Guizhou in southwest China since the last glacial reflected by stalagmite records from Yelang Cave, J. Asian Earth Sci., 114, 549–561, https://doi.org/10.1016/j.jseaes.2015.07.021, 2015.